Ocean Sci. Discuss., 12, 863–895, 2015
www.ocean-sci-discuss.net/12/863/2015/
doi:10.5194/osd-12-863-2015

Ocean Science
Discussions
Open Access

Sunda Shelf Seas: flushing rates and residence times

B. Mayer[1], T. Stacke[2], I. Stottmeister[3], and T. Pohlmann[1]

[1]Institute of Oceanography, University of Hamburg, Bundesstr. 53, 20146 Hamburg, Germany
[2]Max Planck Institute for Meteorology, Terrestrial Hydrology Group, Schäferkampsallee 29, 20146 Hamburg, Germany
[3]Leibniz Institute for Baltic Sea Research, Seestraße 15, 18119 Rostock, Germany

Received: 27 April 2015 – Accepted: 3 May 2015 – Published: 22 May 2015

Correspondence to: B. Mayer (bernhard.mayer@uni-hamburg.de)

Published by Copernicus Publications on behalf of the European Geosciences Union.

Abstract

The region of the Sunda Shelf has an average depth of approx. 48 m and is subject to many physical and biogeochemical processes with a strong impact from human activities. For the investigation of marine environmental water properties and quality, it is helpful to have an idea about exchange rates of water masses in the different parts of this region. Four numerical models, the global hydrodynamical model MPI-OM, the global hydrological model MPI-HM, the regional hydrodynamical model HAMSOM and a Lagrangian tracer model have been utilized to estimate the flushing rates and residence times in different seas on the Sunda Shelf. Using decadal averaged monthly transports, the commonly used flushing rate formula gives rates for the different months of approximately 40 to 70 days for the entire Sunda Shelf. For most parts of it (Malacca Strait, southern South China Sea, Java Sea), the results are similar, while for the Gulf of Thailand, the flushing rates amount to 80 to 170 days. The tracer model provides quite different but very detailed 3-D pictures with residence times of below 30 days to more than two years, depending on the location within the region, on the starting layer and on the season.

1 Introduction

For investigation of marine environments with focus on the local biogeochemical processes, on the impact of marine pollution due to dense coastal human population and on changes of any kind of environmental properties, it is recommendable to have knowledge about hydrodynamical water exchange parameters of the regions of interest, which give an idea about time scales of renewal of the corresponding water bodies. Without this knowledge, it might be difficult to distinguish between different processes inducing changes of water properties (e.g., advection, internal conversions) and to interpret observational or numerical findings.

OSD
12, 863–895, 2015

There are many different types of water exchange parameters mentioned in the literature such as “age”, “flushing rate”, “residence time”, “exposure time”, “transit time”, “turn over time”, “influence time”, “half life time” and so on. Authors like Bolin and Rohde (1973); Zimmermann (1976); Prandle (1984); Takeoka (1984); Luff and Pohlmann (1995); Monsen et al. (2002) and others give different definitions for different time parameters, sometimes even for the same parameters. Some authors define and compare different time parameters (e.g. Prandle, 1984; Monsen et al., 2002; Jouon et al., 2006; Delhez, 2013). Delhez et al. (2004) relate flushing rates to biogeochemical processes and the classification of estuaries.

Certain parameters like the residence time or exposure time are actually Lagrangian properties of each water particle within the domain of interest (Bolin and Rohde, 1973; Zimmermann, 1976; Takeoka, 1984).

For the Indonesian Seas, there are only a few estimations on the renewal of water, they are usually done in connection with investigation of water exchange and water mixing of deep basins (van Aken et al., 1988, 1991; Ffield and Gordon, 1992; Hautala et al., 1996; Qu et al., 2006; Liu et al., 2010; Chang et al., 2010) or to follow the water of the Indonesian Throughflow (ITF) from the Pacific Ocean into the Indian Ocean (Valsala and Ikeda, 2007). Stansfield and Garrett (1997) estimate the flushing rate for the Gulf of Thailand, which is also part of our investigation, to be in the range of half a year with a simple model and based on observed salinity data. Nugrahadi et al. (2013) applied a hydrodynamical Eulerian and a Lagrangian tracer model to the Madura Strait.

The Indonesian Seas are located in a geographical region dominated by two different and opposing wind systems: the summer monsoon lasts from approximately May or June until September with prevailing wind directions from SW to SE, depending on the geographical position, while the winter monsoon with prevailing slightly weaker winds from opposite directions (NE to NW) lasts from November to February or March. The spring and autumn transition periods in between offer highly variable winds in strength and direction while changing their main direction. This meteorological behaviour has

OSD
12, 863–895, 2015

a heavy impact on the ocean circulation. Therefore, we will also focus on the seasonal dependence of the renewal of the water masses in the regions of interest.

A numerical model system was applied to simulate the hydrodynamics as realistic as possible. Our approach for this article is to select certain geographical areas on the shallow Sunda Shelf and calculate their flushing rates τ according to the commonly used formula $\tau = V/Q$ with V being the volume of the water body of the region of interest and Q being the inflowing volume transport through all open boundaries of that region. The results will then be compared with Lagrangian simulation results.

2 Models and methods

2.1 Applied models

A numerical model system has been applied to receive a most realistic distribution of currents, sea surface temperature (SST) and sea surface salinity (SSS). The first component is the global ocean circulation model MPI-OM (Max Planck Institute Ocean Model, Marsland et al., 2003; Jungclaus et al., 2006), the oceanic part of the climate model system used for the IPCC world's climate simulations. It simulated the global ocean circulation on the TP04 grid (Jungclaus et al., 2013), having a horizontal resolution of 24 km (approximately 44 km at lower latitudes) and 40 z layers of increasing thicknesses from top to bottom. Meteorological forcing data were taken from NCEP/NCAR (Kalnay et al., 1996). This model delivered the open boundary forcing data (vertical structure of temperature and salinity, sea surface height) as six hourly time series for the second component of the model system, the regional ocean circulation model HAMSOM (Hamburg Shelf Ocean Model, Backhaus, 1985; Pohlmann, 1996, 2006; Mayer et al., 2010). It covers the area of the Indonesian Seas (90.5 to 134.4° E, 16.5° N to 14.9° S, bathymetry interpolated from the SRTM data (Farr et al., 2007, see Fig. 1) with a horizontal grid resolution of 6 min (approximately 11 km) and 39 z layers with increasing thicknesses from 5 m at the surface to 550 m at greater depths.

OSD
12, 863–895, 2015

The maximum depth was limited to 6260 m. At its open boundaries to the Indian Ocean, the Arafura Sea, the Pacific Ocean and the South China Sea, the aforementioned values from the global model were used, while the atmospheric forcing used the same meteorological data as for the global model. As initial condition for temperature and salinity distribution in the regional domain, the corresponding 3-D distributions were interpolated from MPI-OM results at the time of simulation start.

Finally, freshwater inflow is required at the river mouths. These river runoff data were generated with the MPI-HM (Max Planck Institute Hydrology Model, Stacke and Hagemann, 2012). The MPI-HM is a global hydrological model, which solves the water balance on the land surface. From meteorological forcing data (temperature, precipitation and potential evapo-transpiration) taken from the NCC reanalysis data sets (Ngo-Duc et al., 2005), surface runoff and subsurface drainage are computed. These quantities are routed over the land surface following the predefined river flow network DDM30 (Döll and Lehner, 2002) ending in river mouths, where the fresh water is released into the ocean. The MPI-HM runs at 0.5° resolution with a daily time step. River routing, however, is internally computed at 6 hourly time steps to guarantee numerical stability also for fast flowing rivers. The MPI-HM regularly takes part in model inter-comparison projects (Haddeland et al., 2011; Schewe et al., 2014). The river input points for freshwater in the model topography of the regional model are depicted in Fig. 1 by red dots.

The requested most realistic exchange of fresh water, heat and momentum between ocean and atmosphere limits the thickness of the ocean surface layer. As a consequence, tidal forcing had to be switched off (upper layer thickness is 5 m, tidal range above the Australian Shelf is even more than that). This is unproblematic for two reasons. Firstly, we are rather interested in long-term phenomena and behaviour, where the tides play a minor role. Secondly, the effect of tidal mixing is taken into account by larger horizontal and vertical exchange coefficients. They depend on the shear of the velocity, in HAMSOM and in nature as well. In shallower ocean regions or regions with large topographic gradients, the velocity shear (and the turbulence) is naturally higher, same in the model because of the semi-slip condition at lateral boundaries and bottom

OSD
12, 863–895, 2015

friction. Tides increase the shear more in regions, which have a higher exchange already. This can be simulated by an increased factor in the calculation of the turbulent mixing coefficients. With this, the tidal effect on mixing is roughly included, even though non-linear effects are not. A calibration of the horizontal and vertical exchange factors was performed according to best agreement between simulated and observed velocity components.

The simulation period covered the years 1958 to 2012. Model results were averaged over 24 h.

The fourth component of the model system is a suspended particulate matter transport model (Mayer, 1995; Puls et al., 1997), which was used as a simple Lagrangian tracer model. In this type of model, a particle is placed into the center of each model grid cell being part of the region of interest. The trace of its path and – more important here – the time needed until it leaves the certain region is stored. Since we are interested in following passively the water, we do not take turbulent mixing into account for the tracer drift, only advection plays a role in this case.

2.2 Calculation of water renewal parameters

The regions of interest for the flushing rates and residence times are limited to depths less than 200 m. As shown in Fig. 6, upper left panel, with different semi-transparent shadings, they cover the Gulf of Thailand (red shading), the shallow southern South China Sea (blue shading), the Malacca Strait (green shading), the Java Sea (yellow shading) and the entire Sunda Shelf as the sum of the aforementioned regions. Their geometric properties like average depth, area and volume are listed in Table 1, where the number of 3-D grid cells and with this, the number of particles in the tracer model starting in the corresponding area, is also given.

In order to get a clear idea about the role of the different seasons in this highly variable monsoon-dependent circulation system, the regional model's horizontal velocities were averaged to receive monthly values for each of the five decades from 1960 to

OSD
12, 863–895, 2015

2012 (for the last decade, the years 2010 to 2012 were also added). This procedure enables us to investigate also decadal variability.

With these horizontal velocities, flushing rates $\tau = V/Q$ were calculated for each domain by using the volume of a domain according to Table 1 and the sum of all incoming water transports into the corresponding domain.

For the tracer model simulations, the same decadal monthly averaged 3-D current fields were taken. Four simulations for two years were performed using constant velocities of February, May, August and October of the decade 2000 to 2012 as representatives for the two fully developed monsoon seasons and the transition periods. The residence time was taken as the time needed for a particle to leave the corresponding region of interest for the first time. For the vertical averages displayed in the result pictures, the residence times of the layers were weighted according to the layer thicknesses.

For reasons of clear differentiation of the two applied methods in estimating the renewal rates, we will use the term flushing rate for the analytical calculation and the term residence time for the estimation of the time parameter from the tracer model simulations.

2.3 Validation of the regional model results

For the validation of the model results, comparisons with observed velocities at different key locations within the Indonesian Seas will be presented. Also comparison of sea surface temperature and sea surface salinity with satellite data will show the high quality of the regional model results. For the long-term results, a climatology of the Indonesian Throughflow will underline the capability of the numerical hydrodynamical model system.

OSD
12, 863–895, 2015

2.3.1 Comparison of simulated velocities with moored current meter data

For direct comparison of model results with observed data, measured velocities from moored current meters at different depths of some key locations were used kindly provided by the INSTANT project (International Nusantara Stratification and Transport project, Sprintall et al., 2004, 2009). For 2004 to 2006 at depths 50, 150, 350, 750 m, the time series of simulated daily and observed hourly data are displayed for the locations Labani Channel (Makassar) and Lombok Strait in Fig. 2 and Ombai Strait and Timor Passage in Fig. 3. The locations are shown in Fig. 1. At the end of each graph, diamonds mark the time averaged observed and simulated velocities. For comparison, we should keep in mind that observed data are point measurements, valid actually only for the vicinity of the corresponding depth level, while simulated data represent depth ranges of a model layer, even when they might be interpolated to the requested depth.

Overall, a satisfying agreement can be stated to the time series as well as to the average velocities, which show a slight underestimation by the model at some positions. There are only a few major discrepancies like in the Makassar 350 m curve (peaks in October 2004 and July and August 2006). The Lombok Strait curves for 150 and 350 m show peaks a few days or a week ahead, from which we can conclude that they originate from the Indian Ocean.

Most of these "disturbences" are not locally generated but transferred from the open boundaries into the model domain. Both open boundaries to the Pacific and the Indian Oceans are sometimes – from outside – crossed or touched by strong large gyres or dynamic meandering currents like the South Equatorial Current (SEC), introducing strong horizontal barotropic pressure and density gradients along the open boundaries. Feng and Wijffels (2002) showed strong intraseasonal variations of the SEC in the eastern Indian Ocean, which is located and shifting between 10 and 15° S (and even further), just north of our southern open domain boundary. This is a real challenge for numerical models and can produce artificially high (or low) velocities into or out of the model domain, which can send its signals into the interior of the domain, also

OSD
12, 863–895, 2015

upstream certain currents. This corresponds to signals, different authors found in the Makassar Strait measured data coming in upstream direction from the Lombok Strait and being induced by Kelvin waves in the Indian Ocean (Sprintall et al., 2000; Wijffels and Meyers, 2004; Gordon et al., 2010). Of course, also other signals can travel upstream the Makassar Current.

2.3.2 Comparison of simulated SST and SSS with satellite data

Another presentation of the agreement of simulation results of the regional model HAMSOM with the real condition is a comparison of sea surface salinities (SSS) and temperatures (SST). Both are shown in Fig. 4 including a map for different locations.

For SST comparison, three regions A, B, C have been selected (see map in Fig. 4): (A) a part of the Malacca Strait; (B) the Spermonde Archipelago near Makassar, Sulawesi; (C) an area east of middle-southern Sumatra coast including the Bangka Strait and the Siak river mouth, all for reasons of field work performed during the projects. MODIS (Moderate-resolution Imaging Spectroradiometer) data from both EOS-Aqua and EOS-Terra satellites have been averaged temporally and horizontally over each of these three regions to receive regional monthly time series. MODIS data have an accuracy of 0.4 °C and represent surface squares of 4.6 km × 4.6 km. Simulated SST time series were created by averaging the upper layer model temperature for the same regions and then temporally from daily data. When comparing the time series, we have to keep in mind that the MODIS data are "skin temperatures" (Brown and Minnett, 1999). They are influenced by diurnal solar surface heating and by slight cooling due to evaporation (Minnett, 2003) with a heating effect much stronger than the cooling effect. An average of day and night remote sensing data leads therefore to slightly higher temperature data than the subsurface water would show. The model results are "bulk temperatures" for the model's surface layer with a thickness of about 5 m including the model's water level.

The comparison displayed in Fig. 4 clearly shows that the seasonality as well as the level are in very good agreement, the seasonal peak values are over- or underesti-

OSD
12, 863–895, 2015

mated by no more than 1 K. It has been explained in the previous paragraph that the resulting MODIS averages are slightly higher than subsurface temperature. Therefore, model data are expected to be lower than these remote sensing data.

For SSS comparison, SMOS (soil moisture and ocean salinity sensor) derived data represent – with an accuracy of 0.4 psu – the upper ≈ 1 cm of the ocean surface (Boutin et al., 2014) and horizontal areas of 1° × 1°, averaged from 3 days maps to monthly means. The simulated SSS data are again the values of the upper model layer (5 m thick plus water level), which were taken at the positions indicated in the map of Fig. 4 and averaged to monthly values. The comparing time series are presented in panels 1 to 7 of Fig. 4. Also here, a very good agreement of simulated and observational data is obvious for the level and the seasonal variation if there is any. Differences are usually not more than 1 psu. It is impressive to see the seasonal variation at location 7, eastern Java Sea: During the first and last quarters of a year, the location is effected by relatively fresh water coming from the South China Sea. During boreal summer season, this region is effected by the saltier Makassar Strait throughflow coming more or less directly from the North Pacific Ocean.

A slight overestimation of SSS from the model is expected because of the thickness of the upper layer. Precipitation has a much larger impact on the remote sensing data than on the model data. Since the model does not resolve any vertical profile within the upper 5 m of the ocean, fresh water input from precipitation is immediately mixed into the upper 5 m layer, while the remote sensor detects the fresher water within the upper ≈ 1 cm of the ocean. Because our locations are in the tropical zone with high rain fall rates, we expect the remote sensing data to be rather lower than the model data, which can indeed be seen in the comparing time series of Fig. 4.

2.3.3 Simulated averaged transports through selected sections

Last but not least, the averaged transports through some sections in the Indonesian Seas for the periods 2004 to 2006 and 1970 to 2006 are presented in Fig. 5. For comparison with estimations derived from observations, published values from van

OSD
12, 863–895, 2015

Aken et al. (2009); Sprintall et al. (2009); Gordon et al. (2012) and Feng et al. (2013) are listed in the figure as well.

Also from these transport distributions, we can see a principle agreement of the simulated with expected circulation in the Indonesian Seas according to the cited literature. Remarkable differences are the Ombai Strait and Timor Passage transports, which correspond to the underestimated simulated currents of the comparing time series of the same locations shown in Fig. 3. This is due to the southern part of the eastern open boundary cutting through the Arafura Sea between New Guinea and Australia. Obviously, in the model, a part of the water coming in from the Pacific Ocean leaves through this open boundary instead of recirculating in the Arafura Sea and subsequently leaving the area through Ombai Strait and Timor Passage into the Indian Ocean.

For the Lifamatola Strait, the cited value of −2.5 Sv from van Aken et al. (2009) represents only the depth range below 1250 m, and the authors guess that there is rather a northward transport in upper regions of the passage leading to a total southward transport through this section of even less than 2.5 Sv. Our results of −3.8 Sv, however, correspond to the second cited value, −3.2 Sv, from Feng et al. (2013).

3 Results

3.1 Flushing rates

The results of the analytically calculated flushing rates from the simulated volume transports into the different domains are depicted in Fig. 6. All domains except the Gulf of Thailand are throughflow domains, and with an increasing size of their area and volume, the cross-section of the corresponding open boundaries also increases, which in turn enlarges the possible amount of inflowing water. Probably due to this fact, the flushing rates are similar for all regions except the Gulf of Thailand, ranging from approximately 35 to 65 days, while the Gulf of Thailand is flushed at rates of 75 to 170 days. The latter domain shows the clearest seasonality with lowest flushing rates

OSD
12, 863–895, 2015

in July and August and highest in May and October. For the other domains, the seasonality is weaker with lowest flushing rates in January and highest rates in April to June and in October.

High flushing rates mean low water exchange or slow inflow. During the transition periods between the two monsoon phases, April/May and October, there is some stagnation of the circulation, which partly even changes its direction from one phase to the other. This leads to a deceleration of water currents and longer flushing rates. It has to be noted, if directions of transport change, stagnation is not that obvious for the throughflow domains, because there is inflow on either open side of the domain.

The standard deviation (SD) of the monthly inflowing transports (not shown), which were calculated from daily inflowing transports, range from approximately 9 to 43 % of the monthly mean volume transport depending on the month and the domain, the highest occurring for the Sunda Shelf and the South China Sea. The SD of the flushing rates (also not shown), calculated from daily flushing rates, ranges from 40 up to 300 days with the maxima in the same domains. Obviously, there is a higher intra-monthly than seasonal variability.

There is no decadal trend visible in the monthly results, and the decadal variability is non-specific and low. Inter-annual variability was not investigated because of the well-known general high variability of the current system in the Indonesian Seas (Mayer and Damm, 2012).

3.2 Residence times

The residence times as calculated from the tracer model simulations give us a much more detailed pictures and a quite different impression of the exchange of water in the regions. The model simulated four times a period of two years, forced with constant decadal monthly velocity fields of February, May, August and October, representing the fully developed NW/NE monsoon season, transition period, the fully developed SE/SW monsoon season and the transition period from the last to the first season, respectively.

OSD
12, 863–895, 2015

May instead of April was selected because of the long flushing rates shown in the previous section.

To get an idea about the general order of residence times and the portion of particles (representing the water masses) flushed out after a simulation period of two years, Table 2 lists – for all domains mentioned in the previous flushing rate section – the percentage of particles, which left the corresponding domain after two years, and the half life time of each domain defined as the time needed to flush out 50 % of the particles, which started in the corresponding domain. For direct comparison, the corresponding flushing rates τ are also listed in Table 2.

Prandle (1984) defined a "turn over time" as the time needed to reduce the original uniformly distributed total mass within the region of interest to a factor of e^{-1} or 37 %. For a uniform and constant flow and an immediate redistribution of the remaining mass after a certain amount left the region, this time corresponds exactly to the time we defined as flushing rate. Therefore, looking at the time needed to flush out 63 % would give a comparable measure to the flushing rates. In spite of that, we will compare half life time with flushing rates, because after a two years simulation, even half life time is hardly reached in some regions.

The table shows a great discrepancy to the flushing rates. For May, August and October, most regions have not reached their half life times after two simulation years, while the τ formula calculates flushing rates of mostly two to three months. The entire Sunda Shelf, on which we will focus in this section, reaches a half life time for the February simulation of 472 days ($\approx$ 15 months and three weeks), and during the rest of the second year, $\approx$ 8 months and a week, only 1 % of the remaining water particles are additionally flushed. The flushing rate formula gives a value of 46.3 days. The Java Sea reaches its half life time for the February simulation after 88 days, for August after 144 days, and for October after 184 days, while it is not reached after 2 years in the May simulation. There is no general statement for all regions on the period leading to the fastest water renewal.

OSD
12, 863–895, 2015

The vertically averaged residence times for the region of the entire Sunda Shelf are given for the different seasons in Fig. 7. All panels show values from less than 30 days to more than 2 years (maximum period of simulation) depending on the distance from the entrance or exit of a region and the strength of the circulation. In contrary to the previously calculated flushing rates, most areas show residence times between one and two years. In the February panel, Fig. 7, upper left, we can see a retroflection area or a part of a large gyre at the northeastern entrance to the region with residence times of 3 quarters of a year at the most. The shape of the pattern north of this suggests that an inflow just south of the Vietnamese coast partly turns around to leave the Sunda Shelf area immediately, partly touches the Gulf of Thailand without effecting it. Then, the flow proceeds southward along the West-Malay coast, partly leaves through the Singapore Strait into the Malacca Strait and partly proceeds through the Karimata Strait. One part leaves to the south through the Sunda Strait, another part flows to the east to flush the Java Sea, which is visible from the band of residence times less than 270 days with decreasing values to the east, while the surrounding parts show residence times of more than a year.

During the summer monsoon in August (Fig. 7, lower left panel), these patterns are quite different. The general circulation turned around and shows longer residence times, which is also evident from Table 2. Water movement seems to be slower during this season. In the northeast, we see a distribution indicating a retroflection the other way around than in February. In the Java Sea, the direction of the main flow is also opposite during this season. It is westward with water coming from the Makassar Strait into the Java Sea. The Gulf of Thailand is also effected by the current system and slowly flushed. This general flow is possible, because the winterly meteorological blocking situation stops in April/May and the water masses, which were piled up, are released. Western parts of the near-surface Makassar throughflow can now turn westward into the Java Sea.

In May, after transition from boreal winter to summer monsoon season (Fig. 7, upper right panel), the situation shows similar behaviour like the flushing rates: long resi-

OSD
12, 863–895, 2015

dence times everywhere. But for the Gulf of Thailand, we can see the release of the accumulated water masses in the Gulf during the previous season.

The simulation results for October (Fig. 7, lower right panel) represent the other transition period, also with changing but no prevailing wind directions. The distribution shows even longer residence times than in May indicating a stagnation period, when the main flow direction turns around and the water transport starts to accumulate water masses again in the Indonesian Seas rather than moving through the regions (e.g. Gordon and Susanto, 2001; Mayer and Damm, 2012).

For the Gulf of Thailand as part of the Sunda Shelf region, the residence time in February is simulated mostly with more than two years. Obviously, the inflowing currents retroflect already close to their entrance in a way that there is hardly exchange for central and coastal parts of the Gulf. As mentioned in the previous paragraph, during the boreal winter season, the northerly monsoon winds pile up the water in the southern South China Sea (SCS), which blocks the outflow from the Gulf. Additionally, the southward flow along the Vietnamese coast is topographically hindered from flowing into the Gulf by the Vietnamese most southeastern tip, which directs the flow rather towards the West-Malaysia. The above mentioned band of lower residence times south of Borneo support this interpretation about the flow pattern. The onset of this situation in October shows the same effect for the Gulf area. During the SE monsoon season, the currents obviously intrude further into the Gulf and decrease the residence time to ca. 1.75 to 2 years.

In the Malacca Strait, we can also detect two very different situations, which supports the seasonal flow patterns published already by Mayer and Pohlmann (2014). In February, the distribution shows a relatively fast flowing band along the coast of Sumatra with a direction towards the Andaman Sea. Long residence times south and east of the Singapore Strait indicate this northwest directed flow into and within the Malacca Strait. The above mentioned relatively high water levels produce this flow field. In boreal summer, this extra gradient is relieved, and we have low currents with very high

OSD
12, 863–895, 2015

residence times in the narrow part of the strait but more exchange of water in the wider part, which is transported mainly from the Andaman Sea.

Since we are able to follow the tracers in three dimensions, we can also distinguish the residence times for tracers starting at different depth levels, shown for the upper two and the fourth model layers for the February and August simulations in Fig. 8. The corresponding model layers have thicknesses of 5, 7 and 10 m, representing the depth ranges 0 to 5, 5 to 12 and 22 to 32 m, respectively.

It is interesting to see the very different residence times in the single layer pictures with non-averaged values. In general, the described above features are more obvious. For the surface layer, many areas within the Sunda Shelf region show residence times of less than 30 days to less than half a year. There are some thin lines of long residence times within areas of short residence times. They are caused by particles transported directly to and around islands and then being caught by the "current shadows" behind islands, which extends their time to leave the region.

According to the different residence times for different layers in both simulations and the short residence times in upper layers, the local wind plays a dominant role for the direction and the strength of the water transport in the shallow Sunda Shelf region, while barotropic gradients are of minor importance.

4 Discussion

Two different methods were applied to estimate hydrodynamic time parameters connected with renewal of water body of a certain region, here: the Sunda Shelf and its sub regions: the analytical calculation of the flushing rates and the residence times estimated from tracer model results. The two methods delivered very different results.

The analytical approach of using the formula $\tau = V/Q$ is appropriate only for channel-like or semi-enclosed regions with a rather narrow inlet and a uniform flow field. It is too simple for regions with distinct and diverse circulation patterns. Recirculation of water, which enters the domain (= inflow) but immediately exits the domain due to a small

OSD
12, 863–895, 2015

loop, will alter the results leading to a strong underestimation of renewal times. This is an important point to be considered, as an example, for the investigation of renewal times of water bodies in bays, where sustainable aquaculture is planed and has to be dimensioned to avoid harm to the natural environment.

The application of Lagrangian tracer models to follow water particles and estimate a horizontal or 3-D distribution of the residence times from typical season-averaged flow fields is also not realistic, because there are no monthly averaged situations lasting longer than a month. However, it provides a much better idea about the time ranges for water renewal and a more detailed view on the locations with rather stagnating and rather quickly exchanged water masses. Additionally, it gives us a clearer idea about the influence of the seasons.

The connection between both methods is – for an idealized case of uniform flow and immediate mixing of all remaining with new water – the time reached after exchanging an amount of 63 % of the original water (Prandle, 1984). Instead, we used half life time (exchange of only 50 %), because even this was hardly reached in many regions after the two years simulation. But it clearly shows that both methods deliver results far away from each other with flushing rates of usually less than 100 days and residence times of usually more than 730 days.

For the Indonesian shelf seas, only the tracer model results indicated and visualized that there are big differences in water exchange between locations within the domains of interest and between seasons.

5 Summary and conclusions

For the interdisciplinary investigation of marine environments such as shelf seas, gulfs and bays, it is helpful to have knowledge about basic physical parameters of those regions. One important parameter is the rate of renewal of the water within a certain region, which gives an idea about the importance of external (advective) and internal processes. This is essential for basic environmental research as well as applied in-

OSD
12, 863–895, 2015

vestigations, e.g. for the development of sustainable aquaculture. Two methods were applied to estimate hydrodynamical parameters connected with the process of water renewal within certain regions. From numerical hydrodynamical model results, one method calculated the flushing rates according to the formula $\tau = V/Q$ as the quotient of the volume of a region like the Sunda Shelf and the inflowing water volume transport through all lateral open boundaries. The other method estimated the residence times by applying a Lagrangian tracer model using the same numerical volume transports to follow each water parcel of a region of interest. Results were very different. Especially in case of existing recirculation patterns, the flushing rate calculations immensely underestimate the time needed for water renewal. In contrary, the tracer model application gives a detailed picture concerning the variability in time (seasons) as well as in 3-D space within the region of interest.

Focusing on the entire Sunda Shelf (average depth 49 m), the flushing rate formula gives values between 40 and less than 60 days with low seasonal and decadal variation. The tracer model results give values of 1 to 2 years of residence time for most parts in the region for the vertical average but faster water exchange (residence time less than 1 year) for most parts of the upper three layers (0 to 22 m). Certain areas like the Gulf of Thailand and the Malacca Strait seem to be rather slowly flushed during most time of the year.

In conclusion, the results of the two different methods to estimate the water renewal rates in certain regions recommend the application of Lagrangian tracer models rather than just a calculation with the simple formula. The formula cannot take recirculation patterns into account, which might mislead the investigators towards dramatic underestimations of the times needed under realistic conditions to exchange entire water bodies.

Acknowledgements. This project was funded by the German Ministry of Education and Research under the grant 03F0642D in the frame of the German-Indonesian cooperation SPICE III.

OSD
12, 863–895, 2015

References

Backhaus, J. O.: A three-dimensional model for the simulation of shelf sea dynamics, Deutsche Hydrographische Zeitschrift, 38, 165–187, 1985. 866

Bolin, B. and Rohde, H.: A note on the concepts of age distribution and transit time in natural reservoirs, Tellus, 25, 58–62, 1973. 865

Boutin, J., Martin, N., Reverdin, G., Morisset, S., Yin, X., Centurioni, L., and Reul, N.: Sea surface salinity under rain cells: SMOS satellite and in situ drifters observations, J. Geophys. Res.-Oceans, 5533–5545, doi:10.1002/2014JC010070, 2014. 872

Brown, O. B. and Minnett, P. J.: MODIS Infrared Sea Surface Temperature Algorithm Theoretical Basis Document, Version 2.0, Tech. Rep. Miami, FL 33149-1098, University of Miami, available at: http://modis.gsfc.nasa.gov/data/atbd/atbd_mod25.pdf, 1999. 871

Chang, Y.-T., Hsu, W.-L., Tai, J.-H., Tang, T., and Chang, M.-H.: Cold deep water in the South China Sea, J. Oceanogr., 66, 183–190, doi:10.1007/s10872-010-0016-x, 2010. 865

Delhez, É. J. M.: On the concept of exposure time, Cont. Shelf. Res., 71, 27–36, doi:10.1016/j.csr.2013.09.026, 2013. 865

Delhez, É. J. M., Heemink, A. W., and Deleersnijder, É.: Residence time in a semi-enclosed domain from the solution of an adjoint problem, Estuar. Coast. Shelf S., 61, 691–702, doi:10.1016/j.ecss.2004.07.013, 2004. 865

Döll, P. and Lehner, B.: Validation of a new global 30-min drainage direction map, J. Hydrol., 258, 214–231, doi:10.1016/s0022-1694(01)00565-0, 2002. 867

Farr, T. G., Rosen, P. A., Caro, E., Crippen, R., Duren, R., Hensley, S., Kobrick, M., Paller, M., Rodriguez, E., Roth, L., Seal, D., Shaffer, S., Shimada, J., Umland, J., Werner, M., Oskin, M., Burbank, D., and Alsdorf, D.: The shuttle radar topography mission, Rev. Geophys., 45, RG2004, doi:10.1029/2005RG000183, 2007. 866

Feng, M. and Wijffels, S.: Intraseasonal variability in the south equatorial current of the East Indian Ocean, J. Phys. Oceanogr., 32, 265–277, doi:10.1175/1520-0485(2002)032<0265:IVITSE>2.0.CO;2, 2002. 870

Feng, X., Liu, H. L., Wang, F. C., Wang, F. C., Yu, Y. Q., and Yuan, D. L.: Indonesian throughflow in an eddy-resolving ocean model, Chinese Sci. Bull., 58, 4504–4514, doi:10.1007/s11434-013-5988-7, 2013. 873

Ffield, A. and Gordon, A. L.: Vertical mixing in the indonesian thermocline, J. Phys. Oceanogr., 22, 184–195, doi:10.1175/1520-0485(1992)022<0184:VMITIT>2.0.CO;2, 1992. 865

OSD
12, 863–895, 2015

Gordon, A. L. and Susanto, R. D.: Banda Sea surface-layer divergence, Ocean Dynam., 52, 2–10, 2001. 877

Gordon, A. L., Sprintall, J., van Aken, H. M., Susanto, D., Wijffels, S., Molcard, R., Ffield, A., Pranowo, W., and Wirasantosa, S.: The Indonesian throughflow during 2004–2006 as observed by the INSTANT program, Dynam. Atmos. Oceans, 50, 115–128, doi:10.1016/j.dynatmoce.2009.12.002, 2010. 871

Gordon, A. L., Huber, B. A., Metzger, E. J., Susanto, R. D., Hurlburt, H. E., and Adi, T. R.: South China Sea throughflow impact on the Indonesian throughflow, Geophys. Res. Lett., 39, L11602, doi:10.1029/2012GL052021, 2012. 873

Haddeland, I., Clark, D., Franssen, W., Ludwig, F., Voss, F., Arnell, N., Bertrand, N., Best, M., Folwell, S., Gerten, D., Gomes, S., Gosling, S., Hagemann, S., Hanasaki, N., Harding, R., Heinke, J., Kabat, P., Koirala, S., Oki, T., Polcher, J., Stacke, T., Viterbo, P., Weedon, G., and Yeh, P.: Multimodel estimate of the global terrestrial water balance: setup and first results, J. Hydrometeorol., 12, 869–884, doi:10.1175/2011JHM1324.1, 2011. 867

Hautala, S. L., Reid, J. L., and Bray, N.: The distribution and mixing of Pacific water masses in the Indonesian Seas, J. Geophys. Res., 101, 12375–12389, doi:10.1029/96JC00037, 1996. 865

Jouon, A., Douillet, P., Ouillon, S., and Fraunie, P.: Calculations of hydrodynamic time parameters in a semi-opened coastal zone using a 3D hydrodynamic model, Cont. Shelf. Res., 26, 1395–1415, doi:10.1016/j.csr.2005.11.014, 2006. 865

Jungclaus, J. H., Botzet, M., Haak, H., Keenlyside, N., Luo, J.-J., Latif, M., Marotzke, J., Mikolajewicz, U., and Roeckner, E.: Ocean circulation and tropical variability in the coupled model ECHAM5/MPI-OM, J. Climate, 19, 3952–3972, 2006. 866

Jungclaus, J. H., Fischer, N., Haak, H., Lohmann, K., Marotzke, J., Matei, D., Mikolajewicz, U., Notz, D., and von Storch, J. S.: Characteristics of the ocean simulations in the Max Planck Institute Ocean Model (MPIOM) the ocean component of the MPI-Earth system model, Journal of Advances in Modeling Earth Systems, 5, 422–446, doi:10.1002/jame.20023, 2013. 866

Kalnay, E. Kanamitsu, M., Kistler, R., Collins, W., Deaven, D., Gandin, L., Iredell, M., Saha, S., White, G., Woollen, J., Zhu, Y., Leetmaa, A., Reynolds, R., Chelliah, M., Ebisuzaki, W., Higgins, W., Janowiak, J., Mo, K. C., Ropelewski, C., Wang, J., Jenne, R., Joseph, D: The NCEP/NCAR Reanalysis 40-year project, B. Am. Meteorol. Soc., 77, 437–471, 1996. 866

OSD
12, 863–895, 2015

Liu, Y., You, Y., Bao, X., and Wu, D.: The flushing and exchange of the South China Sea derived from salt and mass conservation, Deep-sea research. Part 2, Topical studies in oceanography, Deep-Sea Res. Pt. II, 57, 1212–20, doi:10.1016/j.dsr2.2009.12.010, 2010. 865

Luff, R. and Pohlmann, T.: Calculation of Water Exchange Times in the ICES-Boxes with a Eulerian Dispersion Model using a Half-Life Time Approach, German Journal of Hydrograohy, 47, 287–299, 1995. 865

Marsland, S. J., Haak, H., Jungclaus, J. H., Latif, M., and Röske, F.: The Max-Planck-Institute global ocean/sea ice model with orthogonal curvilinear coordinates, Ocean Model., 5, 91–127, 2003. 866

Mayer, B.: A threedimensional numerical SPM transport model with application to the German Bight, in: GKSS Report 95/E/59, edited by: GKSS Forschungszentrum Geesthacht GmbH, GKSS, 96 pp., 1995 (in German). 868

Mayer, B. and Damm, P. E.: The Makassar Strait throughflow and its jet, J. Geophys. Res., 117, C07020, doi:10.1029/2011JC007809, 2012. 874, 877

Mayer, B. and Pohlmann, T.: Simulation of organic pollutants: first step towards an adaptation to the Malacca Strait, Asian Journal of Water, Environment and Pollution, 11, 75–86, available at: http://iospress.metapress.com/content/00705368j784503w, 2014. 877

Mayer, B., Damm, P. E., Pohlmann, T., and Rizal, S.: What is driving the ITF? An illumination of the Indonesian throughflow with a numerical nested model system, Dynam. Atmos. Oceans, 50, 301–312, doi:10.1016/j.dynatmoce.2010.03.002, 2010. 866

Minnett, P. J.: Radiometric measurements of the sea-surface skin temperature: the competing roles of the diurnal thermocline and the cool skin, Int. J. Remote Sens., 24, 5033–5047, doi:10.1080/0143116031000095880, 2003. 871

Monsen, N. E., Cloern, J. E., Lucas, L. V., and Monismith, S. G.: A comment on the use of flushing time, residence time, and age as transport time scales, Limnol. Oceanogr., 47, 1545–1553, doi:10.4319/lo.2002.47.5.1545, 2002. 865

Ngo-Duc, T., Polcher, J., and Laval, K.: A 53-year forcing data set for land surface models, J. Geophys. Res., 110, D06116, doi:10.1029/2004jd005434, 2005. 867

Nugrahadi, M. S., Duwe, K., Schroeder, F., and Goldmann, D.: Seasonal variability of the Water Residence Time in the Madura Strait, East Java, Indonesia, Asian Journal of Water, Environment and Pollution, 10, 117–128, 2013. 865

Pohlmann, T.: Predicting the thermocline in a circulation model of the North Sea, Part 1: Model description, calibration and verification, Cont. Shelf. Res., 16, 131–146, 1996. 866

OSD
12, 863–895, 2015

Pohlmann, T.: A meso-scale model of the central and southern North Sea: consequences of an improved resolution, Cont. Shelf. Res., 26, 2367–2385, 2006. 866
Prandle, D.: A modelling study of the mixing of 137Cs in the seas of the European Continental Shelf, Philos. T. R. Soc. A, 310, 407–436, available at: http://www.jstor.org/stable/37423, 1984. 865, 875, 879
Puls, W., Heinrich, H., and Mayer, B.: Suspended particulate matter budget for the German Bight, Mar. Pollut. Bul., 34, 398–409, doi:10.1016/S0025-326X(96)00161-0, 1997. 868
Qu, T. D., Girton, J. B., and Whitehead, J. A.: Deepwater overflow through Luzon Strait, J. Geophys. Res.-Oceans, 111, C01002, doi:10.1029/2005JC003139, 2006. 865
Schewe, J., Heinke, J., Gerten, D., Haddeland, I., Arnell, N. W., Clark, D. B., Dankers, R., Eisner, S., Fekete, B. M., Colón-González, F. J., Gosling, S. N., Kim, H., Liu, X., Masaki, Y., Portmann, F. T., Satoh, Y., Stacke, T., Tang, Q., Wada, Y., Wisser, D., Albrecht, T., Frieler, K., Piontek, F., Warszawski, L., and Kabat, P.: Multimodel assessment of water scarcity under climate change, P. Natl. Acad. Sci. USA, 111, 3245–3250, doi:10.1073/pnas.1222460110, 2014. 867
Sprintall, J., Gordon, A. L., Murtugudde, R., and Susanto, R. D.: A semiannual Indian Ocean forced Kelvin wave observed in the Indonesian seas in May 1997, J. Geophys. Res., 105, 17217–17230, doi:10.1029/2000JC900065, 2000. 871
Sprintall, J., Wijffels, S., Gordon, A. L., Ffield, A., Molcard, R., Susanto, R. D., Soesilo, I., Sopaheluwakan, J., Surachman, Y., and van Aken, H. M.: INSTANT: new international array to measure the Indonesian throughflow, EOS T. Am. Geophys. Un., 85, 369–376, 2004. 870
Sprintall, J., Wijffels, S. E., and Molcard, R.: Direct estimates of the Indonesian throughflow entering the Indian Ocean: 2004–2006, J. Geophys. Res., 114, 1–58, 2009. 870, 873
Stacke, T. and Hagemann, S.: Development and evaluation of a global dynamical wetlands extent scheme, Hydrol. Earth Syst. Sci., 16, 2915–2933, doi:10.5194/hess-16-2915-2012, 2012. 867
Stansfield, K. and Garrett, C.: Implications of the salt and heat budgets of the Gulf of Thailand, J. Mar. Res., 55, 935–963, doi:10.1357/0022240973224184, 1997. 865
Takeoka, H.: Fundamental concepts of exchange and transport time scales in a coastal sea, Cont. Shelf. Res., 3, 311–326, 1984. 865
Valsala, V. K. and Ikeda, M.: Pathways and effects of the Indonesian throughflow water in the Indian Ocean using particle trajectory and tracers in an OGCM, J. Climate, 20, 2994–3017, available at: http://search.proquest.com/docview/222915841?accountid=105241, 2007. 865

OSD
12, 863–895, 2015

van Aken, H. M., Punjanan, J., and Saimima, S.: Physical Aspects of the flushing of the East Indonesian Basins, Neth. J. Sea Res., 22, 315–339, doi:10.1016/0077-7579(88)90003-8, 1988. 865

van Aken, H. M., van Bennekom, A. J., Mook, W. G., and Postma, H.: Application of munk abyssal recipes to tracer distributions in the deep waters of the South-Banda Basin, Oceanol. Acta, 14, 151–162, available at: http://tinyurl.sfx.mpg.de/u2vb, 1991. 865

van Aken, H. M., Brodjonegoro, I. S., and Jaya, I.: The deep-water motion through the Lifamatola Passage and its contribution to the Indonesian throughflow, Deep-Sea Res. Pt. I, 56, 1203–1216, doi:10.1016/j.dsr.2009.02.001, 2009. 872, 873

Wijffels, S. E. and Meyers, G.: An intersection of oceanic waveguides: variability in the indonesian throughflow region, J. Phys. Oceanogr., 34, 1232–1253, doi:10.1175/1520-0485(2004)034<1232:AIOOWV>2.0.CO;2, 2004. 871

Zimmermann, J. T. F.: Mixing and flushing of tidal embayments in the western Dutch Wadden Sea Part I: Distribution of salinity and calculation of mixing time scales, Neth. J. Sea Res., 10, 149–191, doi:10.1016/0077-7579(76)90013-2, 1976. 865

OSD
12, 863–895, 2015

Table 1. Some geometric data about the flushing regions: their number of horizontal grid points and 3-D grid cells in the regional model, their average depth, their area and their volume.

no	name of region	2-D grid points	3-D grid cells	avr depth [m]	area [km^2]	volume [km^3]
1	Sunda Shelf	15 396	89 063	48.8	1 893 307	92 374
2	Gulf of Thailand	2587	13 606	41.7	315 437	13 161
3	Malacca Strait	1131	6726	50.6	139 330	7052
4	South China Sea*	7652	48 454	55.4	942 625	52 173
5	Karimata Strait	1806	7609	31.2	223 234	6970
6	Java Sea	3543	17 907	40.3	436 274	17 576

* Here, South China Sea means only the Sunda Shelf part of South China Sea. All regions are shown in Fig. 6, upper left panel.

OSD
12, 863–895, 2015

Table 2. Percentage of particles flushed out of the regions and half life times (hlt, number of days to flush out 50 % of the particles) after a simulation period of two years with constant velocity fields of climatological February, May, August and October. Third column of each month is flushing rate τ.

name of region	Feb			May			Aug			Oct		
	out [%]	hlt [day]	τ [day]	out [%]	hlt [day]	τ [day]	out [%]	hlt [day]	τ [day]	out [%]	hlt [day]	τ [day]
Sunda Shelf	49.7	> 730	46.4	37.8	> 730	61.5	41.5	> 730	54.2	34.5	> 730	60.3
Gulf of Thailand	17.0	> 730	138.4	29.3	> 730	178.5	27.9	> 730	93.8	21.2	> 730	162.1
Malacca Strait	44.9	> 730	48.3	49.4	> 730	63.3	38.7	> 730	70.0	54.2	327	61.7
South China Sea*	65.7	97	38.2	52.2	352	66.2	39.6	> 730	48.1	44.1	> 730	57.2
Karimata Strait	77.8	32	30.5	46.3	> 730	41.8	63.8	47	33.4	72.5	69	44.3
Java Sea	68.6	92	56.3	43.1	> 730	84.0	62.7	139	62.0	62.0	201	76.6

* Here, South China Sea means only the Sunda Shelf part of South China Sea. All regions are shown in Fig. 6, upper left panel.

OSD
12, 863–895, 2015

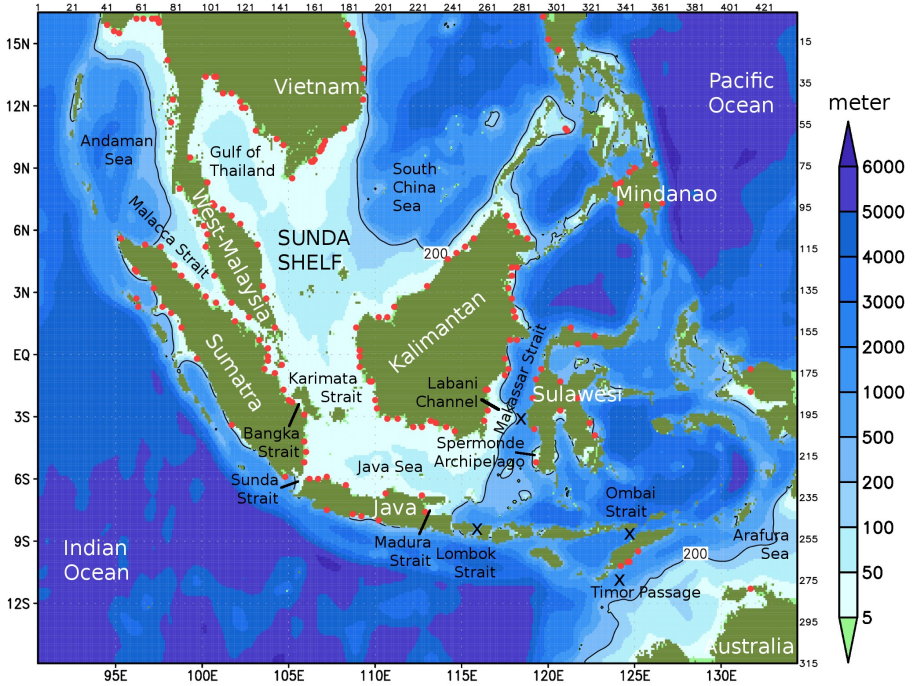

Figure 1. Regional hydrodynamical model domain with bathymetry. Red dots: river input points; X: locations of four moorings for comparison of simulated and observed data. Isobath of 200 m is also drawn to depict the Sunda Shelf limit. Along the upper and right axes, model grid indices are shown.

OSD
12, 863–895, 2015

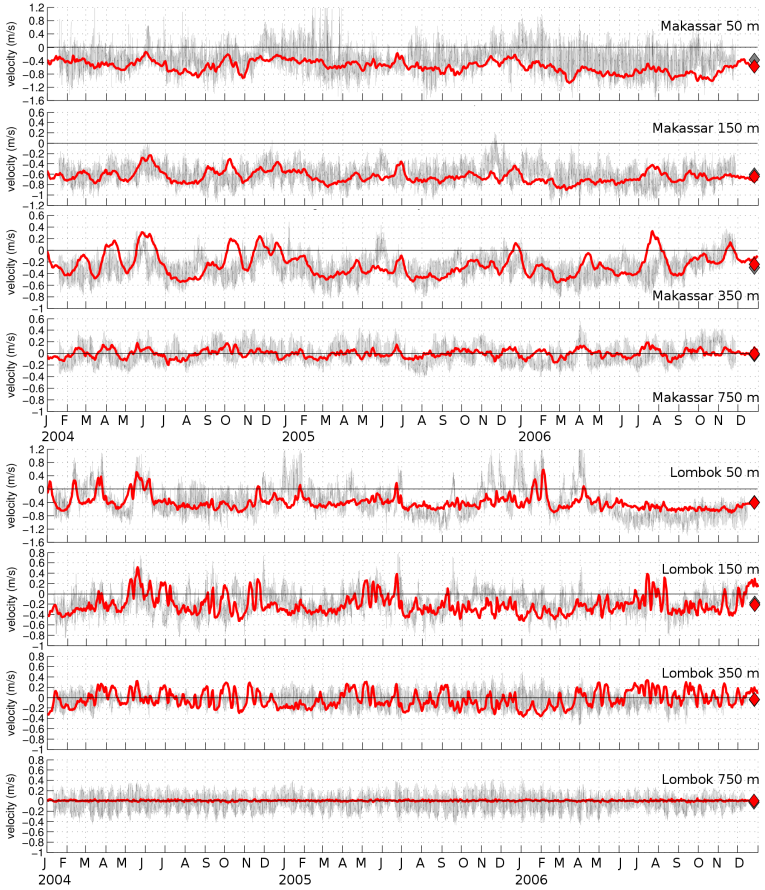

Figure 2. Comparison of simulated (red) and measured (gray) meridional velocities in Labani Channel (Makassar) and Lombok Strait (see Fig. 1) at different depths for 2004 to 2006. Diamonds at end of graphs show mean values.

OSD
12, 863–895, 2015

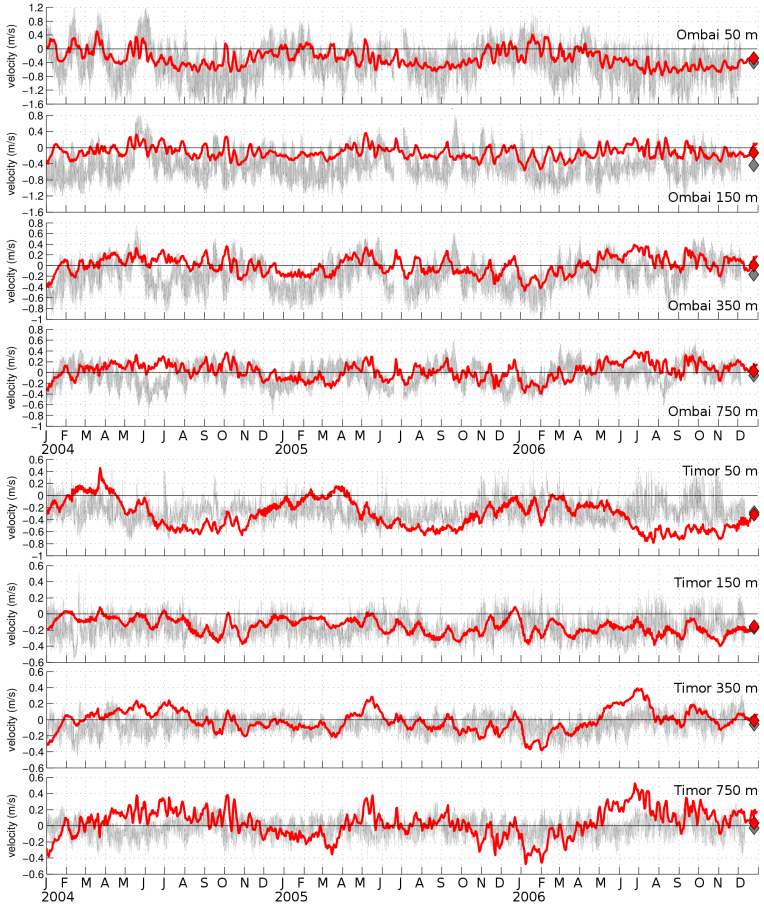

Figure 3. Comparison of simulated (red) and measured (gray) zonal velocities in Ombai Strait and Timor Passage (see Fig. 1) at different depths for 2004 to 2006. Diamonds at end of graphs show mean values.

OSD
12, 863–895, 2015

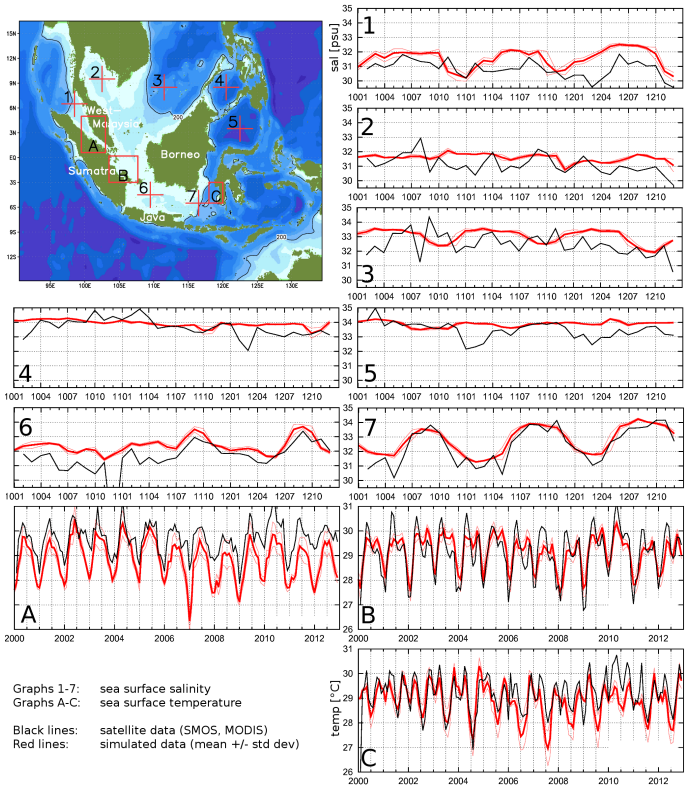

Figure 4. Simulated and satellite observed sea surface salinity (SSS) and temperature (SST) at different positions. Satellite SSS is from SMOS for 2010 to 2012, satellite SST from MODIS Aqua and Terra for 2000 to 2012.

OSD
12, 863–895, 2015

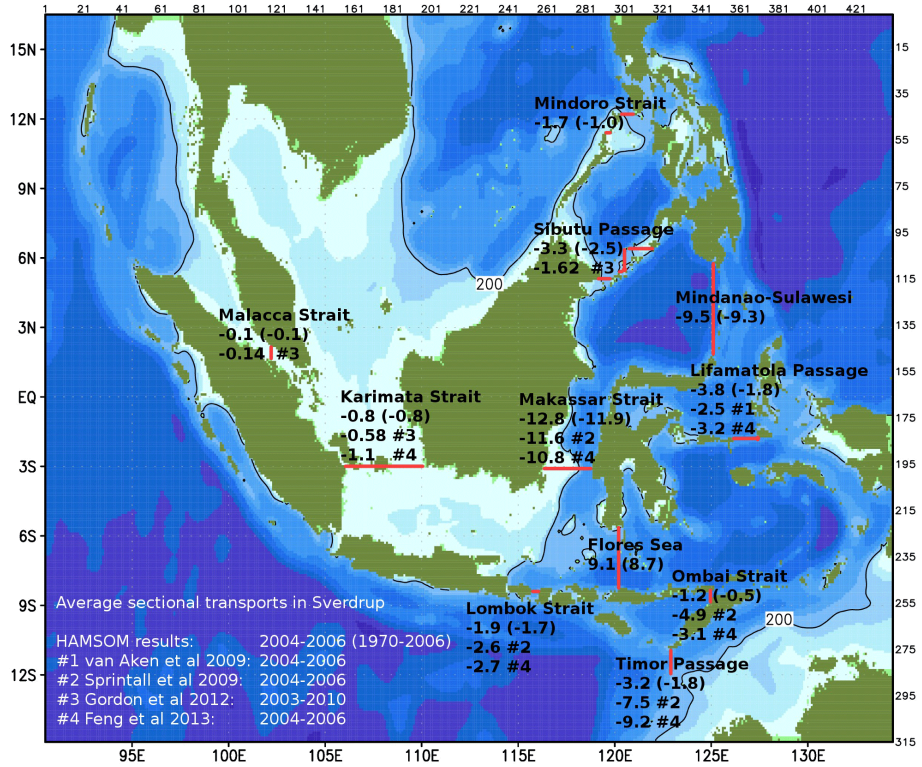

Figure 5. Simulated and literature referenced averaged transports through different sections for periods 2004 to 2006 and – in brackets – 1970 to 2006 in Sverdrup (= 10^6 m^3 s^{-1}), positive is north- or eastward, negative south- or westward. Upper lines display always the simulated and lower lines the cited values.

OSD
12, 863–895, 2015

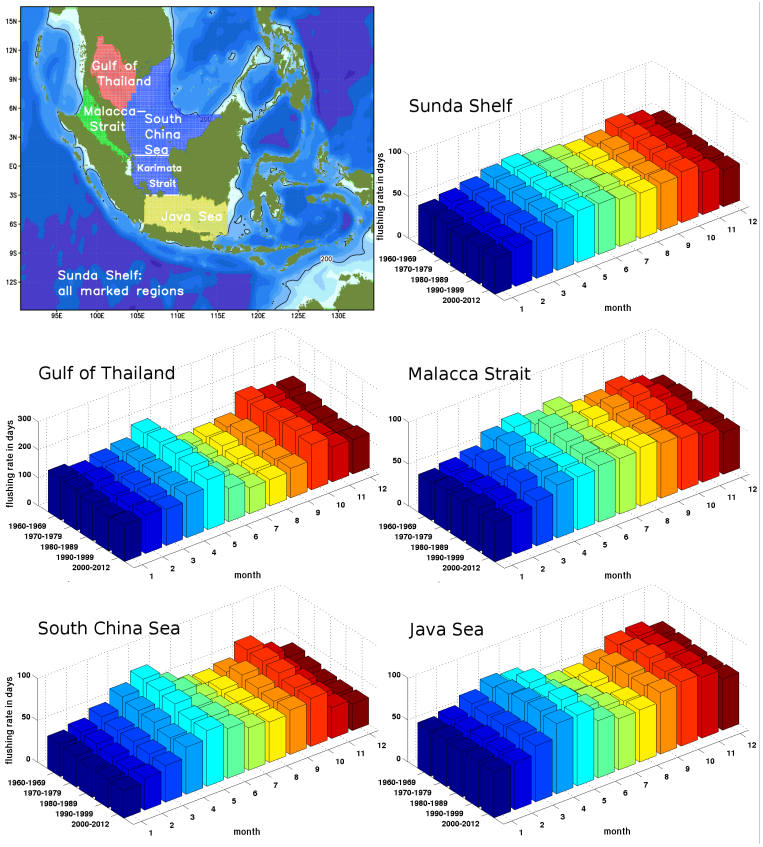

Figure 6. Flushing rates for different regions on the Sunda Shelf in days. Regions are indicated in upper left panel.

OSD
12, 863–895, 2015

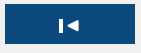

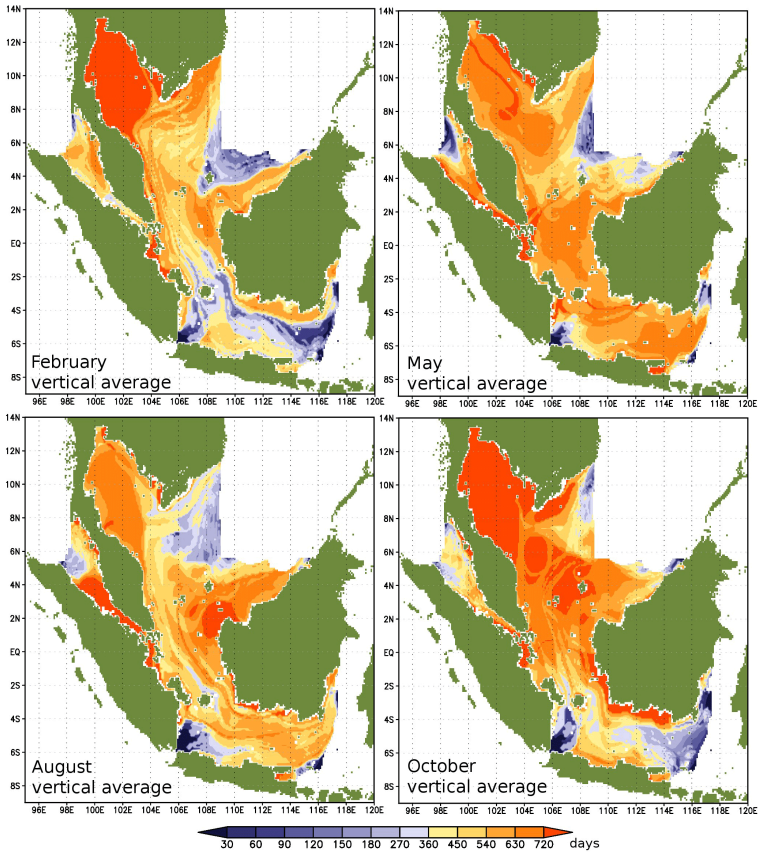

Figure 7. Residence times as simulated by the tracer model for region Sunda Shelf for 2000 to 2012 monthly mean velocity fields of February, May, August and October.

OSD
12, 863–895, 2015

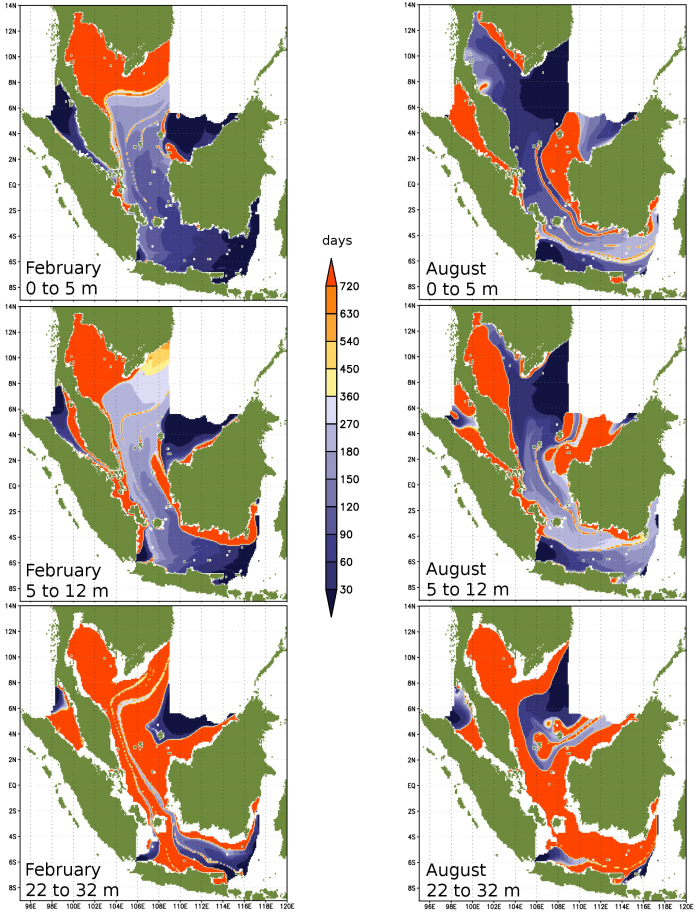

Figure 8. Residence times as simulated by the tracer model for three model layers of the Sunda Shelf region for 2000 to 2012 monthly mean velocity fields February and August.

OSD
12, 863–895, 2015